

# Biologically Inspired Visual Odometer for Navigation of a Flying Robot

Fumiya Iida  
Artificial Intelligence Laboratory  
Department of Information Technology  
University of Zurich  
*Winterthurerstr. 190, CH-8057 Zurich, Switzerland*  
E-mail : iida@ifi.unizh.ch

## Abstract

The ability to navigate in a complex environment is crucial for both animals and robots. Particularly flying insects are capable of surprisingly good navigation despite the small size and relative simplicity of their brains. Recent experimental research in biology has uncovered a number of different ways in which insects use cues derived from optical flow for navigational purposes, such as safe landing, obstacle avoidance and dead reckoning. In this study, we use a synthetic methodology to gain additional insights into the navigation behavior of bees, specifically focus on the mechanisms of course stabilization behavior and visually mediated odometer for the purpose of long distance goal-directed navigation. On the basis of a biology model of motion detector, we propose mechanisms for course stabilization behavior and visual odometer, and evaluate its performance with the blimp type flying robot platform in uncontrolled indoor environments. The result shows that the proposed mechanism can be used to provide an estimate of the distance traveled, but the performance depends on the route the robot follows. Further analysis is also conducted in order to improve the performance of the proposed method.

**Keywords:** Insect navigation, Robot navigation, Visual odometer, Elementary Motion Detector

## 1. Introduction

Navigation in complex 3-D environments is very challenging for both animals and robots. Because of the limited weight capacity and potentially hazardous conditions, the control systems of flying machines are mostly highly complex, where a lot of sensory systems are generally required, such as GPSs, gyroscopes, compasses, ultrasonic sensors, inclinometers, accelerometers, and laser rangefinders [1][4][6]. Compare to flying machines, however, flying insects solve this task in a robust and adaptive manner despite their tiny brain. Behavioral studies with insects have revealed that a number of important navigational abilities rely mainly on visual information: more specifically, image motion induced by ego-motion plays a crucial role in the navigational tasks. Navigation using biologically inspired optical flow has been investigated mainly on land-based agents. The basic behaviors observed in flying insects, e.g. obstacle avoidance, fixation behaviors, were demonstrated with relatively simple mechanisms [5][9]. Owing to its simplicity, such mechanisms have been incorporated in a robot exclusively using analog hardware [5]; a VLSI implementation has been also realized [12]. In a similar way, simulated flying agents were used for altitude control and obstacle avoidance [10][11][12], and a robotic gantry demonstrated the landing behavior of flies [17].

In addition to such basic behaviors, however, mechanisms for long distance navigation are crucial for such insects as honeybees, which navigate accurately and repeatedly from their hive to a food source. This type of navigation normally requires that both directional and distance information be available. Whereas in direction estimation, there is a lot of evidence that celestial cues and especially the polarization pattern of the sky play crucial role [7], the way that bees gain information about the distance traveled has been a point of dispute for many years. Behavior study with honeybees have recently uncovered a mechanism behind visually mediated

odometry, in which the primary cue is the integral, over time, of the image motion that is experienced en route. Given these biological background, in this paper, we propose a biologically inspired navigation method using visual odometry model in combination with a course stabilization mechanism, and test its performance by using a freely flying robot we developed.

In the following section, we introduce navigation mechanisms of flying insects in detail. In section 3, we propose a visual odometry model and explain the experiments with an autonomous flying robot in section 4. Further issues are discussed in section 5.

## 2. Insect Navigation

The vision systems of flying insects are exquisitely sensitive to motion, because visual motion induced by ego-motion can tell the animal much about its own motion and also about the structure of its environment. Behavior experiments with flies and bees show a number of different ways in which insects use cues derived from optical flow for navigational purposes (for review, see [14]). Early studies showed that a tethered fly inside a striped drum tends to turn in the direction in which the drum is rotated [13]. This reaction, so-called optomotor response, serves to help the insect maintain a straight course by compensating for undesired deviations.

For the purpose of long distance goal-directed navigation, recent studies of bees' behavior suggested that the amount of image motion plays an important role in estimating the distance traveled [15]. Early studies suggested that the distance is gauged in terms of total energy consumption during a foraging journey, but recent studies of the bees' behavior questioned this hypothesis, and suggested that visual cues, more specifically the amount of image motion, play an important role on estimating the distance traveled [15][16][18]. In these studies, bees were initially trained to search for the food source in the vertically striped tunnel. Then the searching behavior of the trained bees was observed when the pattern of stripes on the walls was changed, by using different stripe periods, different width between right and left walls, and walls with horizontal stripes. With horizontal stripes, bees tend to fail searching for the food source at the right location, therefore it was concluded that vertical stripes are used for the visual odometer. With different period of stripes, bees succeed in finding the food source position, which implied that bees measure the distance independent of the spatial frequency of the stimulus in the environment. However, when the distance to both walls was increased or decreased compared to the training situation, bees tend to fail in searching at the right location. The main conclusion from these studies was that the bee's visual odometer provides an estimate of distance that is independent of the spatial frequency of the visual stimulus, i.e., it only depends on the angular velocity of the image projected on the insect's retina.

On the basis of above mentioned behavioral experiments as well as electrophysiological studies, a model of motion detection in the insect's nervous system, the Elementary Motion Detector (EMD), has been proposed (for review, see [2]). A well-known model of the EMD is the so-called Reichardt detector, which belongs to a class of correlation-type detectors, shown in Figure 1. Two adjacent photoreceptors send their outputs to temporal high-pass filters that remove constant illumination containing no motion information. These signals are then "delayed" by exploiting the phase lag inherent in a first order temporal low-pass filter. While not a true time delay, the low-pass filter is a good approximation that biology appears to use. Delayed channels are then correlated with adjacent, non-delayed channels by means of a multiplication operation. Finally the outputs of two opponent EMDs are subtracted to yield a strongly direction-sensitive response. Although the nature of the neural mechanisms and the location in the visual pathway remains to be elucidated, some behaviors of the motion sensitive neurons in insects can be well characterized by this motion detector model [14]. The salient properties of the movement-sensitive mechanism underlying these responses are that it is directional, and it does not encode the speed of the moving image. Rather, it is sensitive to the

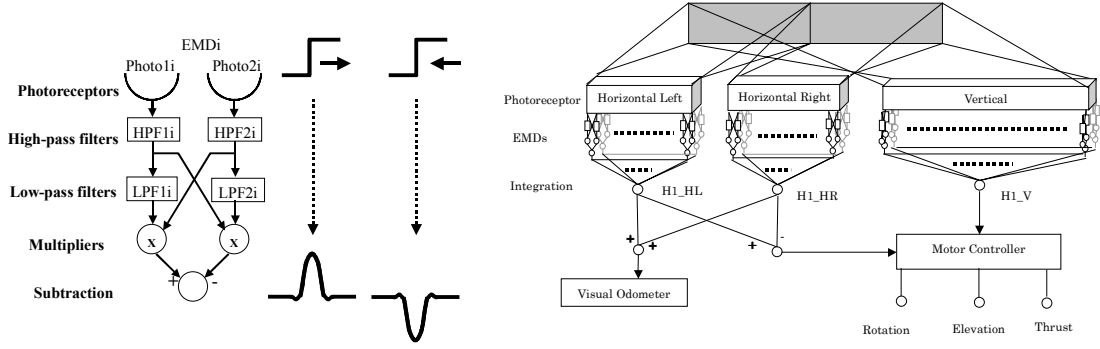


**Figure 1. Left:** the Reichardt model of elementary motion detection. Photoreceptors, high-pass filters, low-pass filters, multipliers, and the subtraction module are wired in series. The output of the last step (subtraction) is an estimate of direction sensitive image speed. **Right:** The controller circuit for the flying robot and visual odometer. The gray rectangle denotes the panoramic image extracted from the omni-directional camera on the robot. The image is given to both horizontally and vertically arranged photoreceptor arrays of EMDs. After the integrators and comparator, the outputs are given to a motor controller and visual odometry module.

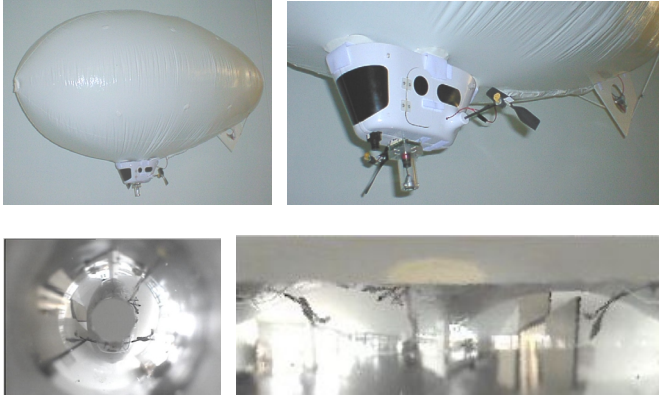


**Figure 2 Top:** The autonomous flying robot, Melissa and its gondola, on the bottom of which a miniature panoramic camera attached. **Bottom:** An image obtained by the panoramic vision system (left) and its log-polar transformed image (right), which is used in the experiments.

temporal frequency of intensity fluctuations generated by the moving image, and therefore confounds the speed of the image with its spatial structure.

On the basis of these biology studies, in the following sections, we propose models of course stabilization and visual odometer, which is evaluated by the experiments with a freely flying robot.

### 3. Navigation Experiments of a freely flying robot

#### 3.1 Course Stabilization Behavior

Inspired from flying insects' course stabilization behavior, which is characterized by fixation behavior using optomotor response, we propose course stabilization model for a flying robot. Figure 1 illustrates the control procedure: At first, image from panoramic vision system (see next section for details) are log-polar transformed, whose intensity information is given to the 3 2 dimensional EMD arrays, i.e. Horizontal Left (HL), Horizontal Right (HR), and Vertical (V). These arrays extract horizontal motion from the left and the right lateral images, and vertical motion from the whole image, respectively. The outputs of each EMD array are then integrated in order to simulate the wide field motion sensitive interneurons H1:

$$H1\_HL(t) = \sum_i \sum_j EMD\_HL_{ij}(t) \quad (1)$$

$$H1\_HR(t) = \sum_i \sum_j EMD\_HR_{ij}(t) \quad (2)$$

$$S_{\text{rotation}}(t) = H1\_HL(t) - H1\_HR(t) \quad (3)$$

To estimate the rotational ego-motion of the robot, the right and left horizontal motions are

compared by simple subtraction. Vertical motion, i.e. changes in height, is estimated by Vertical 2 dimensional EMD array, in which EMDs are vertically arranged. The outputs are integrated as  $S_{altitude}$ :

$$S_{altitude}(t) = H1\_V(t) = \sum_i \sum_j EMD\_V_{ij}(t) \quad (4)$$

These rotation and height sensory information induced by ego-motion is then given to a motor controller module. The 3 parameters are required for the control of the flying robot (see the next section for the details), i.e. rotation, elevation and thrust motor control, which are determined by the following equation.

$$\begin{bmatrix} M_R \\ M_E \\ M_T \end{bmatrix} = \begin{bmatrix} W_{RS} & 0 & 0 \\ 0 & W_{ES} & 0 \\ 0 & 0 & W_{bias} \end{bmatrix} \cdot \begin{bmatrix} S_{rotation} \\ S_{altitude} \\ 1 \end{bmatrix} \quad (5)$$

where  $M_R$ ,  $M_E$  and  $M_T$  are the rotation, elevation, and thrust motor outputs of robot, respectively. In this motor controller, thrust motor rotates at constant speed.

### 3.2 Visual Odometry

For the visual odometry, we re-use the same Horizontal EMD arrays that are also used for course stabilization control (Figure 1). Since the EMD response provides an angular velocity signal (more exactly, a spatio-temporal signal that depends on the speed of the stimulus as well as its spatial frequency), the distance traveled could be estimated by integrating the EMD outputs over time. The responses from both right and left horizontal EMD arrays are integrated every time step, which is given to the visual odometer module, then accumulated over time. Namely the visual odometer response,  $\mathbf{VO}$ , is calculated by integrating the  $\mathbf{H1\_HL}$ ,  $\mathbf{H1\_HR}$  output over time:

$$\mathbf{VO} = \sum_t \mathbf{H1\_HR}(t) + \mathbf{H1\_HL}(t) \quad (6)$$

## 4. Experiment

### 4.1 Method

To evaluate the performance of our model, we developed an autonomous flying robot, shown in Figure 2. The flying robot Melissa is a blimp-like flying robot, which consists of a helium balloon, a gondola hosting the onboard electronics, and a host computer. The balloon is 2.3m long and has a lift capacity of approximately 500g. Inside the gondola, there are 3 motors for elevation and thrust control (a motor for rotation control is attached directly to the balloon), a four-channel radio link, a miniature panoramic vision system, and the batteries. The panoramic mirror has a hyperbolic surface that provides a visual field of 360 degrees on the horizontal plane and 260 degrees vertically. The control process of Melissa can be decomposed to three basic steps. First, the video signal from the CCD camera attached to the gondola is transmitted to the host computer via a wireless video link. Second, the images are then digitized on the host computer, which also performs the image processing in order to determine the target motor command. And third, the motor command is sent to the gondola also via radio transmission. The frame rate of the visual processing is set to 10.0 fps constantly. The robot uses 180 (horizontal) x 60 (vertical) pixels (90 x 30 EMDs), which covers 360 degrees along horizontal plane and 120 degrees along vertical plane in the panoramic image homogeneously, i.e. angular distances between photoreceptors, the sampling bases, are 1.0 degree. The  $W$  matrix of the equation (5) is heuristically determined before experiments, since it is strongly dependent on the hardware conditions (floating balance of the robot etc.) and environment factors (air currents etc.). Three

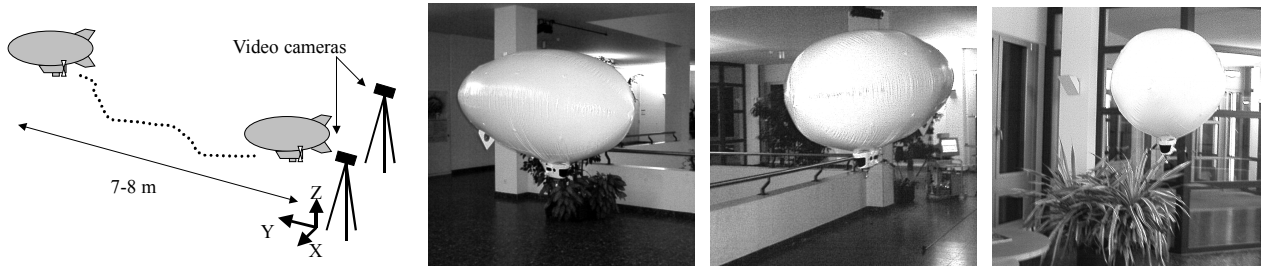


**Figure 3** **Left:** Experimental setup for the navigation experiments. The experiments start with the same initial conditions, i.e. initial robot position and orientation. Two video cameras are installed to record the absolute trajectory of the robot for later analysis. **Right:** Pictures of three different uncontrolled environments, which are tested in the experiments. (EXP 0, 1, 2, from left to right)

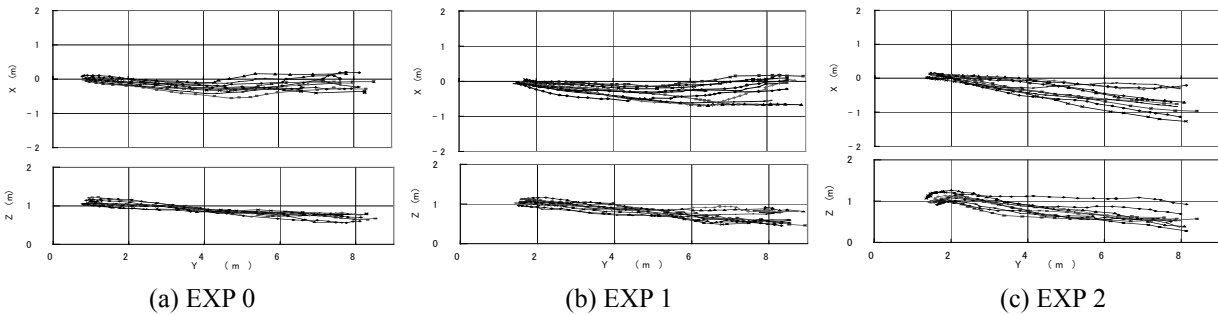


**Figure 4.** 3-D trajectories of the flying robot during the experiments. Each plot is extracted from the images recorded with the stereo video camera. The plots denotes the position of the robot at one second time-step, and each graph shows the trajectories of 10 trials.

sets of experiments are conducted in three different uncontrolled indoor locations (EXP0, EXP1 and EXP2 shown in Figure 3), where we installed two video cameras to track and record the absolute trajectory of the robot for later analysis (Figure 3). Each set of experiment consists of 10 flight trials: in one trial, the robot starts controlling at the same conditions, i.e. initial position, initial orientation, and stops after the same time duration. Due to the limitation of the experimental environments, the time durations are set to 25 seconds.

## 4.2 Results

In Figure 4, the plots show 3-D coordinates of the robot in one-second steps, which are extracted from two external video camera images. In these graphs, each trial starts from left toward right. Since the proposed course stabilization model does not have a specific fixed target location, but simply maintains a straight route determined by the initial orientation of the robot, a small initial difference of the robot orientation results in a relatively large deviation of the goal position, as shown in the X-Y plane figures of EXP 1 and 2. However, most of the trajectories show that the robot maintain the straight routes. For the altitude control, height is eventually maintained in a certain range in all of the trials, although the robot tends to lose the height at the beginning of experiments.

Figure 5 shows the visual odometer responses that the robot obtains during each trial. The visual odometer measures almost the same distances in each experimental setup, EXP 0, 1, and 2. Nevertheless, there seem to be a correlation between the X-Y route deviations in Figure 4 and the visual odometry deviations. For the quantitative analysis of this correlation, the standard deviations of the final odometer responses are calculated (Table 1), in which, first, the odometry output of each trial is divided by the corresponding actual distance, then second, the standard deviations are calculated as percent of mean values (SD). The minimum SDs are 6.8% in EXP 0 and 1, whereas the result from EXP2 is high deviations, which implies that spatial structures of the experimental environment significantly affect the final visual odometer outputs, since, on the one hand, the robot navigates in the different locations in each EXP 0, 1, and 2, and on the other

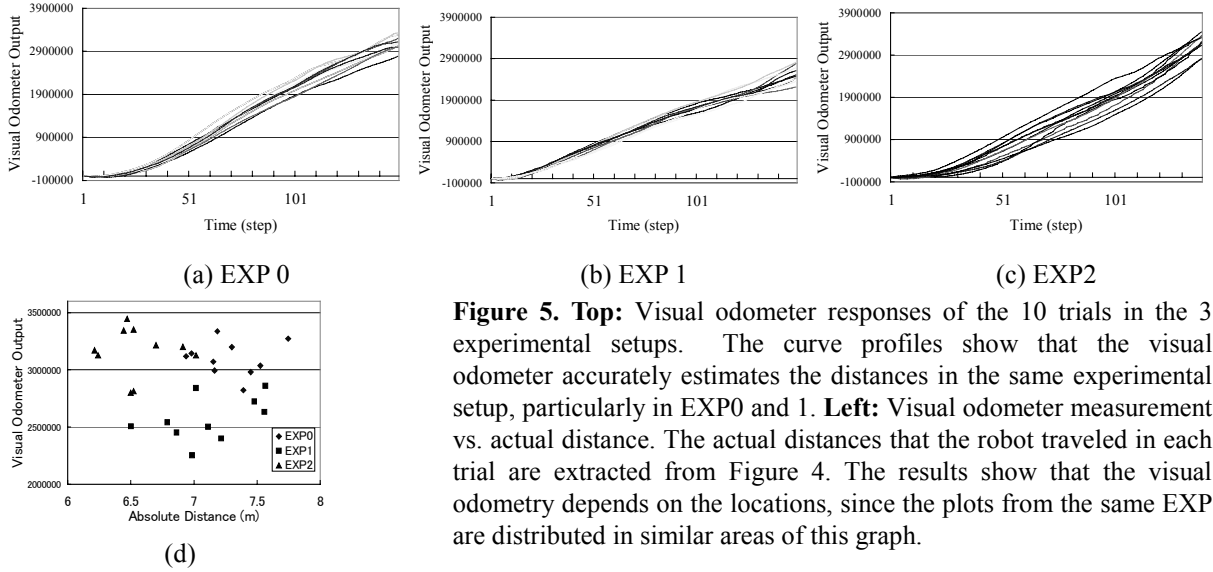


**Figure 5. Top:** Visual odometer responses of the 10 trials in the 3 experimental setups. The curve profiles show that the visual odometer accurately estimates the distances in the same experimental setup, particularly in EXP0 and 1. **Left:** Visual odometer measurement vs. actual distance. The actual distances that the robot traveled in each trial are extracted from Figure 4. The results show that the visual odometry depends on the locations, since the plots from the same EXP are distributed in similar areas of this graph.

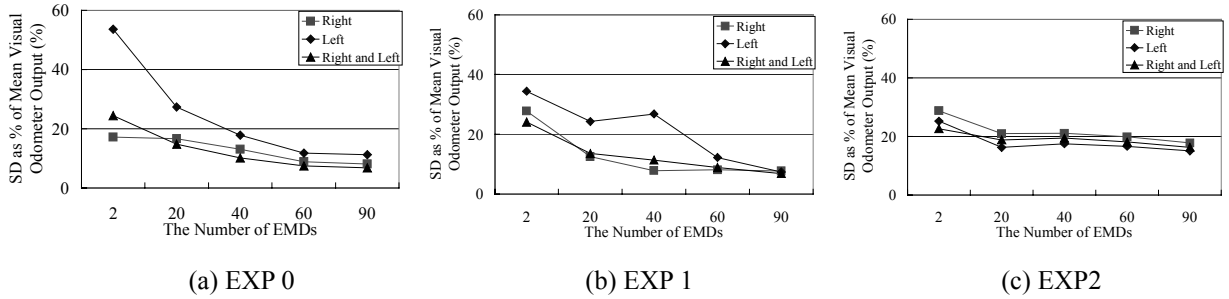


**Figure 6.** The effect of the number of EMDs by standard deviations (SD) as percent of the mean values in visual odometry measurement. The graphs show that the number of EMDs changes the accuracy of visual odometry measurements.

**Table 1.** Standard Deviations as percent of mean values of the visual odometer outputs (VO) and the actual distance the robot traveled (AD).

	EXP 0	EXP 1	EXP 2
VO	3.44	4.95	3.94
AD	6.81	6.86	16.29

hand, the route deviations of EXP 2 in Figure 4 is also large, although the standard deviations of the actual distances are relatively small (Table 1). Furthermore, the visual odometer responses are plotted against the corresponding actual distances in Figure 5(d), where the actual distances are estimated from the externally observed 3D trajectories shown in Figure 4. The results from each EXP0, 1 and 2 tend to distribute in a similar area in this figure, i.e. the EXP 0 plots distribute in the upper right, EXP 1 in the bottom, EXP 2 in the upper left area, which suggests that the odometry measurement would be dependent on the locations of the experiments.

Further analyses are conducted with respect to the effects of the number of EMDs. In this analyses, from the stored data of EMD outputs, we re-calculated the visual odometer outputs by using the different number of EMDs: 1, 10, 20, 30, and 45 EMDs are selected over each left and right laterally distributed EMDs, then integrated their outputs over time. These results are again normalized by the actual distances, and their standard deviations are plotted in Figure 6 as percent of the mean values. There are two implications that should be mentioned. Firstly, in principle, one EMD is essentially the minimum requirement of the proposed visual odometry model, although redundancy improves the measurement errors for all EXP 0, 1, and 2. Secondly, the numbers of EMDs required for the visual odometer depend on the environment, since the

curve profiles of SDs are different in each experiment, as shown in Figure 6. For example, in EXP1 and EXP2, the standard deviations of both right and left visual fields are significantly larger than either right or left ones. Moreover, in EXP 2, the performance is not significantly improved in the case of more than 20 EMDs. From these results, depending on the environment, there would be specific visual fields that are able to estimate the distance more reliably than others, which suggests that there is a possibility to increase the performance of the proposed visual odometer model by adaptively changing areas of EMDs used for the visual odometer.

## **5. Discussion**

### ***5.1 Course stabilization***

In our experiments, we take advantage of the optomotor control for the yaw rotational control, instead of yaw, roll, and pitch controls of flying insects. However the mechanism we employed can be applicable to all three rotational controls in case of the other robotic platforms with an omni-directional vision. For the altitude controls, in this paper, we employed the vertical EMDs to measure the vertical image movement. It is relatively easy in our robotic platform, because, in principle, it has almost no motion induced by roll and pitch rotations. In the case of other robotic platforms, it requires a compensation mechanism for these roll and pitch motions, because they also produce vertical motions. However such motions can be distinguished from the vertical translation motion with direction-sensitive motion detectors, since the opposite side of visual fields has always motions in the other direction: e.g. for roll motion, right motion is going down, but left motion going up, and vice versa. Measuring the ground speed could be an alternative mechanism to control altitude. For example, the robot can exploit the physical constraints of the slower apparent ground speed when the robot flies at higher altitude. It has been reported that flies use such a constraint to control altitude and height at the same time in the landing process [17].

### ***5.2 Visual odometry***

There are some potential solutions to improve the performance of the proposed visual odometer model. Since the above mentioned experimental results show that the performance of the visual odometer relies significantly on the spatial structure experienced during the navigation, and this course stabilization mechanism is potentially prone to vulnerable against unanticipated deviations, one solution would be to minimize route deviations. Considering that celestial cues would play an important role of global compass in natural system, compass information would improve the performance. According to the results above, however, the combination of course stabilization behavior and visual odometer would be a redundant backup. Alternatively, as suggested in Figure 6, the EMD locations of the visual field need to be carefully considered for the better performance of the visual odometer, especially in unstructured environments. More accurate speed control would be another solution, since, in our experiment, thrust control was simply fixed to the constant speed, although the EMD is sensitive to the spatio-temporal frequency. According to a number of experiments with bees, visual odometry would be based on a pure speed detector, rather spatio-temporal filters such as the EMDs employed in this paper, although mechanisms of such a pure speed detectors are still remained to be elucidated.

## **6. Conclusion**

This paper presents a biologically inspired visual odometer mechanism in combination with course stabilization behavior based on an EMD model in the context of goal-directed navigation framework of bees. We performed experiments using a blimp-type robot platform in unstructured indoor environments, and the proposed model successfully demonstrates to estimate the distance the robot traveled. In addition, the further analysis shows that the redundancy in sensory system plays an important role for the robust performance of the visual

odometry measurement, which leads to some possible solutions for the improvement of the proposed model.

## Acknowledgements

This work is supported by the Swiss National Science Foundation, grant no 2000-061372.00, and the Swiss Federal Office for Education and Science (VIRGO TMR network, BBW-No. 96.0148).

## References

- [1] Amidi O., Kanade T., and Fujita K., "A Visual Odometer for Autonomous Helicopter Flight," *Intelligent Autonomous Systems*, Y. Kakazu et al. (Eds.), IOS Press, pp.123-130, 1998.
- [2] Borst A., Egelhaaf M., "Detecting visual motion: Theory and models, *Visual Motion and its Role in the Stabilization of Gaze*," Eds. F.A. Miles and J. Wallman, Elsevier Science, pp. 3-27, 1993
- [3] Chahl J. S., Srinivasan M. V., "Reflective surfaces for panoramic imaging," *Applied Optics*, vol. 36, No. 31, pp. 8275-8285, 1997
- [4] Fagg A. H., Lewis M. A., Montgomery J. F., Bekey, G. A., "The USC Autonomous Flying Vehicle: an Experiment in Real-Time Behavior-Based Control," *IEEE/RSJ International Conference on Intelligent Robots and Systems (IROS)*, Yokohama, Japan, pp. 1173-80, 1993
- [5] Franceschini N., Pichon J. M., Blanes, C., "From insect vision to robot vision," *Phil. Trans. R. Soc. Lond. B*, 337, pp. 283-294, 1992
- [6] Fürst S., Dickmanns E. D., "A vision based navigation system for autonomous aircraft," *Intelligent Autonomous Systems*, Y. Kakazu et al. (Eds.), IOS Press, pp.765-774, 1998
- [7] Gould, J. L., Gould, C. G., *The Honey Bee*, Scientific American Library, New York, 1988
- [8] Harrison R. R., Koch C., "A neuromorphic visual motion sensor for real-world robots," *Workshop on Defining the Future of Biomorphic Robotics, IROS'98*, 1998
- [9] Huber S. A., Franz M. O., Bülthoff H. H., "On robots and flies: Modeling the visual orientation behavior of flies," *Robotics and Autonomous Systems* 29, Elsevier, pp.227-242, 1999.
- [10] Mura F., Franceschini N., "Visual control of altitude and speed in a flying agent," *Proceedings of 3rd international conference on Simulation of Adaptive Behavior: From Animal to Animats III*, pp.91-99, 1994
- [11] Netter T., and Franceschini N., "Towards nap-of-the-earth flight using optical flow," *Proceedings of ECAL99*, pp. 334-338, 1999
- [12] Neumann T. R., Bülthoff H. H., "Insect Inspired Visual Control of Translatory Flight," J. Kelemen and P. Posik (Eds) *ECAL2001 LNAI2159 Springer Verlag* , pp. 627-636, 2001
- [13] Reichardt W., "Movement perception in insects," In W. Reichardt (Eds.), *Processing of optical data by organisms and machines*, pp.465-493, New York: Academic, 1969.
- [14] Srinivasan M. V., Poteser M., Kral K., "Motion detection in insect orientation and navigation," *Vision Research* 39, pp. 2749-2766, 1999
- [15] Srinivasan M. V., Zhang S., Altwein M., and Tautz J., "Honeybee Navigation: Nature and Calibration of the "Odometer"," *Science*, vol. **287**, pp. 851-853, 2000.
- [16] Srinivasan M. V., Zhang S. W., and Bidwell N., "Visually mediated odometry in honeybees," *Journal of Experimental Biology*, 200, pp. 2513-2522, 1997
- [17] Srinivasan M. V., Zhang S. W., Chahl J. S., Barth E., Venkatesh S., "How honeybees make grazing landings on flat surfaces," *Biol. Cybern.* 83, pp.171-183, 2000.
- [18] Srinivasan M. V., Zhang S. W., Lehrer M., Collett T. S., "Honeybee navigation en route to the goal: visual flight control and odometry," In *Navigation* (ed. R. Wehner, M. Lehrer and W. Harvey). *Journal of experimental Biology*. 199, pp. 155-162, 1996